Perspective on the physics of two-dimensional perovskites in high magnetic field (F)

(iD) **Alessandro Surrente**, (iD) **Michał Baranowski, and** (iD) **Paulina Plochocka**

COLLECTIONS

(F) This paper was selected as Featured

View Online   **Export Citation**   **CrossMark**

ARTICLES YOU MAY BE INTERESTED IN

Recent advances in flexible thermoelectrics
Applied Physics Letters **118**, 170503 (2021); https://doi.org/10.1063/5.0049451

Optoelectronic intelligence
Applied Physics Letters **118**, 160501 (2021); https://doi.org/10.1063/5.0040567

Materials, physics, and devices of spin–orbit torque effect
Applied Physics Letters **118**, 180401 (2021); https://doi.org/10.1063/5.0054652
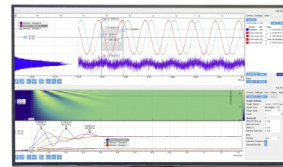
Perspective on the physics of two-dimensional perovskites in high magnetic field Ⓕ

View Online   Export Citation   CrossMark

Alessandro Surrente,[1] 🆔 Michał Baranowski,[1] 🆔 and Paulina Plochocka[1,2,a] 🆔

AFFILIATIONS

[1]Department of Experimental Physics, Faculty of Fundamental Problems of Technology, Wroclaw University of Science and Technology, Wroclaw 50-370, Poland

[2]Laboratoire National des Champs Magnétiques Intenses, UPR 3228, CNRS-UGA-UPS-INSA, Grenoble 38042, France and Laboratoire National des Champs Magnétiques Intenses, UPR 3228, CNRS-UGA-UPS-INSA, Toulouse 31400, France

[a]Author to whom correspondence should be addressed: paulina.plochocka@lncmi.cnrs.fr
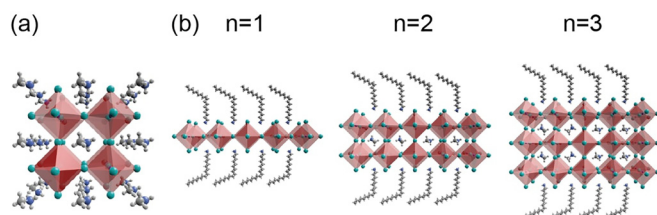
ABSTRACT

Two-dimensional (2D) metal halide perovskites consist of atomically thin layers composed of low bandgap metal-halide slabs, surrounded by high bandgap organic ligands, which behave as barriers. In this Perspective, we highlight how the use of large magnetic fields has been an extremely insightful tool to unravel some of the fundamental electronic properties of 2D perovskites. We focus on the combination of magnetoabsorption measurements and theoretical modeling to extract the carrier effective mass, on the use of magnetic field to clarify the fine structure of the exciton manifold, and on how magnetic fields can be helpful to correctly assign side peaks in the complex absorption or photoluminescence spectra displayed by 2D perovskites. We finally point out some challenges which might be successfully addressed by magneto-optical experimental techniques.

The term perovskite designates any solid which shares the same crystal structure as calcium titanate,[1] and is generically described by the formula ABX_3. The corresponding crystal structure, shown schematically in Fig. 1(a), comprises corner-sharing octahedra BX_6, which compose the inorganic backbone of the crystal, and an A cation, which fills the voids between the octahedra. Metal halide perovskites are direct bandgap semiconductors in which the A site is occupied by an organic or inorganic cation and the B site is generally occupied by Pb

FIG. 1. Schematic crystal structure of (a) a bulk metal halide perovskites and of (b) two-dimensional perovskites with inorganic slabs consisting of $n = 1$, 2, 3 lead halide planes.

or Sn. Finally, the octahedra vertices are occupied by halide anions, such as Cl, Br, or I. Even though the burgeoning research activity on this class of materials is relatively recent,[2] the first synthesis of a metal halide perovskite compound was reported in 1893,[3] followed almost a century later by the first hybrid organic–inorganic semiconducting perovskite.[4] The cation included in the A site has a strong impact on the crystal structure of the resulting material. If its size is sufficiently small to be accommodated between the octahedra, as is the case for small organic [methylammonium (MA), formamidinium (FA)] or inorganic [cesium (Cs)] cations, then the crystal structure will be a periodic repetition in the three dimensions of the inorganic backbone represented in Fig. 1(a). These materials are often referred to as three-dimensional (3D) or bulk perovskites. If the A site cation is substantially larger than the space between the octahedra (as in the case of large organic molecules consisting of aliphatic or aromatic chains), it will violate the Goldschmidt tolerance factor,[5] which leads to the formation of crystals consisting of thin slabs of lead-halide octahedra, surrounded by large organic molecules which act as spacers, as illustrated schematically in Fig. 1(b). These materials are informally referred to as two-dimensional (2D) or layered perovskites and belong to the Ruddlesden–Popper (RP)[6,7] or Dion–Jacobson (DJ)[8] phase. The

general formula describing RP 2D perovskites is $(A)_2A'_{n-1}MX_{3n+1}$, where A represents a large organic monovalent cation (ended with an amine group, NH_3), which acts as a spacer between inorganic octahedral slabs.[9] In the case of DJ phase,[8] the organic spacer is a divalent cation ended from both sides by amine groups: $(A)A'_{n-1}MX_{3n+1}$, where A' is a small cation (MA, FA, Cs).

Initially, 2D perovskites have been intensively investigated for their fundamental electronic properties as they can be considered as an "ideal and natural quantum well," where charge carriers are confined in the central lead-halide slab, while the organic spacers act as barriers[10] and they are not plagued by interface roughness or the intermixing characteristic of epitaxially grown quantum wells. Moreover, a significant mismatch between the dielectric constant of the organic and inorganic moieties[11] leads to a considerable reduction of the dielectric screening of the Coulomb interaction between the photocreated electron-hole pairs. 2D perovskites have been the first system where theoretical studies on Coulomb correlation in ultrathin films[12,13] could be tested experimentally.[14] The strong reduction of the dielectric screening leads to tightly confined excitonic complexes, with binding energies on the order of hundreds of millielectronvolts.[14–16] Subsequently, layered perovskites were used as the charge transport material in transistor devices.[17,18] The rise of bulk perovksites as one of the most promising materials for photovoltaic applications[2] and the simultaneous wide scientific interest in layered materials such as graphene,[19] transition metal dichalcogenides,[20] hexagonal boron nitride,[21] and their heterostructures,[22,23] has led to a rediscovery of 2D perovskites. Their better environmental stability[24–27] as compared to their 3D counterparts[28,29] has been used to protect 3D perovskites in a heterojunction geometry.[30] However, 2D perovskites are now intensively investigated as materials in their own right, with applications in light emitting diodes,[31,32] lasers,[33,34] white light emitters,[35,36] high efficiency solar cells,[25,37] photodetectors,[38,39] and polaritonic devices.[40] Their electronic and optical properties can be tuned by acting on a variety of knobs, such as their thickness,[6] the organic spacers,[14,41,42] which also enable a certain degree of control over the dielectric confinement,[16] the composition,[43,44] and the thickness of the metal-halide slab.[6,15] Importantly, the choice of the organic spacer can influence the distortion of the inorganic sublattice,[45] which, in turn, has a considerable impact on the optical properties of the 2D perovskites by changing the coupling between charge carriers and lattice vibrations.[41,46–50] Thus, 2D perovskites offer a vast playground to explore extremely rich physics where the electronic and lattice properties are intertwined.

The investigation of the optical response of 2D perovskites under high magnetic field represents a powerful experimental tool to achieve a thorough understanding of their electronic properties and to disentangle the effects of the different degrees of freedom listed above. Optical spectroscopy in high magnetic field can be considered a conceptually simple experimental technique, which yields straightforward information about charge carrier effective masses, their g-factors, the spatial extension of the exciton wave function, and the energy structure of the exciton levels. These quantities are in turn of high importance for practical applications or are fed into theoretical models, which makes magneto-optical spectroscopy one of the workhorses of semiconductor physics.

In this Perspective, we summarize the progress in the understanding of the fundamental electronic properties of 2D perovskites revealed by magneto-optical spectroscopy. Magneto-optical measurements are experimentally challenging in the case of layered perovskites due to their very high exciton binding energies[15] and low carrier mobility.[51–53] In order for the effects of magnetic field to be experimentally detectable, usually very large magnetic fields (up to $\gtrsim 100$ T) are required. In the first part of this Perspective, we describe how magnetic field is the only direct and straightforward experimental technique which has allowed a reliable and accurate determination of the exciton reduced mass in metal halide perovskites. Later, we comment shortly on how the use of high magnetic field can help study the coupling between charge carriers and phonons. Subsequently, we describe how magnetic field can be used to unveil the energy structure of excitonic complexes. In final part, we highlight research directions which can potentially benefit from the use of high magnetic fields.

The carrier effective mass is one of the most fundamental parameters, directly connected to the band structure and involved in a wide variety of phenomena, which include the charge transport and optical absorption. It directly or indirectly influences the operation of semiconductor devices. The experimental determination of the effective mass relies on a variety of experimental techniques, some among which are based on the use of magnetic field. Magnetic field-related phenomena such as Shubnikov-de Haas oscillation[54] or magnetophonon resonances[55] are directly connected to the effective mass. Also magneto-optical spectroscopy provides a direct handle to the effective mass. The carrier cyclotron resonance (or, in other words, intraband transitions between Landau levels) observed in the THz or far infrared spectral range allows the independent determination of the hole[56] or electron[57] effective mass. Also magneto-optical spectroscopy performed in the visible or near infrared spectral range can be very informative. It can provide directly quantitative information on the exciton binding energy,[58] size of exciton wave function, and reduced mass μ. In an experimental approach conceptually similar to THz magneto-optical spectroscopy, if cyclotron resonance experiments are performed in the visible or near infrared spectral range, which corresponds to excitonic and band to band transitions, the exciton reduced mass can be measured directly and accurately.[59–63] So far, virtually all of the attempts to determine band structure parameters of 2D and 3D perovskites have been based on the optical spectroscopy of the interband transition in very high magnetic fields.[15,41,64–67] This can be understood as a consequence of low carriers mobility in perovskites[51–53] and their ambipolar character, which hinders measurements by means of transport or THz techniques. The first magneto-optical studies of 2D perovskites focused on the magnetic field dependence of the excitonic transitions.[68–70] In the weak field limit, the characteristic energy related to the Coulomb interaction, represented by the exciton binding energy, is much larger than the cyclotron motion energy. In the Faraday configuration, with the magnetic field parallel to the light wave vector, and in the weak field limit, the shift of the excitonic transition has two components:

$$E_X(B) = \pm \frac{1}{2} g\mu_B B + c_0 B^2, \quad (1)$$

where g is the Landé g-factor, μ_B is the Bohr magneton, and c_0 is the diamagnetic coefficient. The linear contribution is related to the Zeeman splitting; the quadratic dependence is referred to as diamagnetic shift. Due to the very large exciton binding energy in 2D perovskites[15] (as in other layered materials[71,72]) even for magnetic fields of few tens of teslas, the diamagnetic approximation of Eq. (1) is valid, as
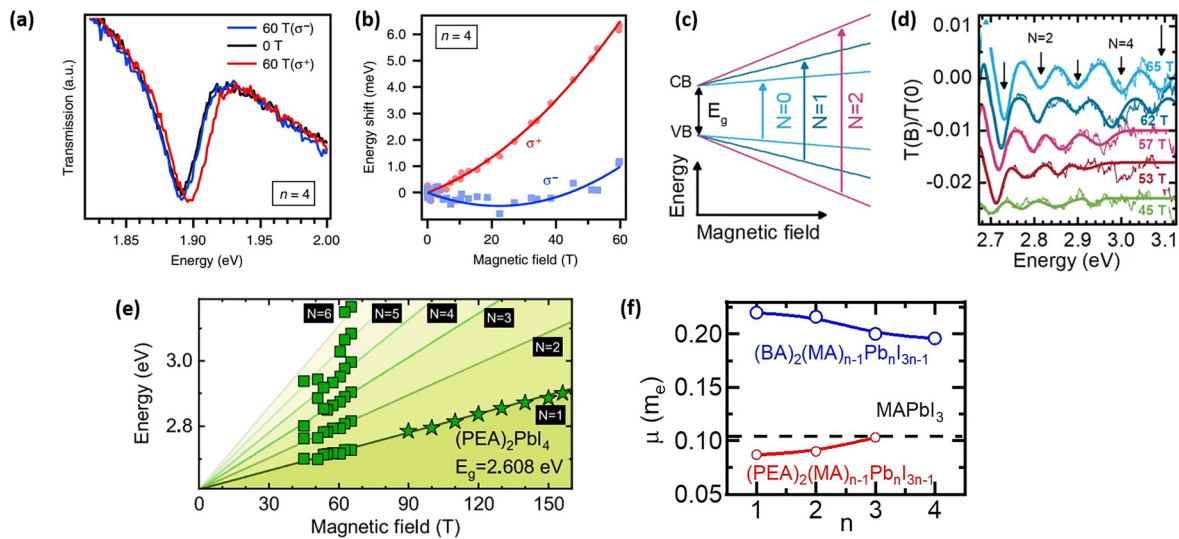
FIG. 2. (a) Transmission spectra of a $(BA)_2(MA)_3Pb_4I_{13}$ crystal for right- and left-handed circular polarization with (red and blue) and without (black) magnetic field. (b) Corresponding shift of the exciton energy as a function of the magnetic field together with fits with Eq. (1). (a) and (b) Adapted with permission from Blancon et al., Nat. Commun. 9, 2254 (2018). Copyright 2018 Author(s), licensed under a under Creative Commons Attribution 4.0 License.[15] (c) Schematic showing the allowed optical transitions between the Landau states in the conduction (CB) and valence (VB) band as a function of the magnetic field. (d) $T(B)/T(0)$ ratioed transmission spectra at different magnetic fields B. Arrows indicate equally spaced absorption minima corresponding to interband Landau level transitions. (e) Fan chart showing the measured energy of the interband Landau transitions as a function of the applied magnetic field at 2 K for $(PEA)_2PbI_4$. (c)–(e) Adapted with permission from Dyksik et al., ACS Energy Lett. 5, 3609–3616 (2020).[66] Copyright 2020 American Chemical Society. (f) Dependence of the carrier reduced mass μ for BA-[15] and PEA-based[67] 2D perovskites as a function of n.

demonstrated by the magnetoabsorption spectra of Fig. 2(a) and by the parabolic trend of the transition energy vs magnetic field shown in Fig. 2(b).[15] The diamagnetic coefficient c_0 depends on the exciton effective mass and on the spatial extension of the exciton wave function:[73]

$$c_0 = \frac{e^2}{8\mu}\langle r^2\rangle \sim \frac{\epsilon^2}{\mu^3}, \qquad (2)$$

where e is the elementary charge, μ is the reduced exciton mass, and $\langle r^2\rangle$ is the mean square value of the in-plane spatial extension of the exciton wave function. Initial studies reported different values of the diamagnetic coefficient for 2D perovskites, consisting of a single lead halide octahedra plane, ranging from 7×10^{-8} eV/T^2 (Ref. 70) to 3.5×10^{-7} eV/T^2.[69] The recently revived interest in 2D perovskites led to a significant number of magneto-optical studies on samples with different organic spacers, which resulted in more systematic values of the diamagnetic coefficient and exciton reduced mass, summarized in Table I.

Unfortunately, the knowledge of the diamagnetic coefficient alone does not allow us to determine the reduced mass of exciton. This is because the spatial extension of the wave function depends not only on the effective mass, but also on the dielectric screening and quantum confinement. To derive a quantitative estimate of the effective mass from the diamagnetic coefficient, a model of the exciton has to be assumed. In the case of 2D perovskites, characterized by a strong difference between the dielectric constant of the inorganic wells and the organic barriers,[75] the 2D hydrogenic model,[69] the Keldysh potential,[76] image charge effect,[74] or more complex models based on first principles calculations[15,77] can be found in the literature.

Nevertheless, some important conclusions can be drawn from the measurements of the exciton diamagnetic shift. Based on an

advanced modeling of the exciton wave function, it has been shown that the exciton reduced mass can be substantially modified by increasing the thickness of the inorganic quantum well.[15] For the series of $(BA)_2(MA)_{n-1}$ Pb_nI_{3n+1} structures with $n = 1, 2, 3...$ (where BA stands for buthylammonium, MA for methylammonium cations and n indicates the number of inorganic layers), the diamagnetic coefficient was reported to systematically increase with increasing n (see

TABLE I. Experimentally determined diamagnetic coefficients c_0 and exciton reduced masses μ for a variety of 2D perovskite compounds. BA, butylammonium; HA, hexylammonium; OA, octylammonium; DA, decylammonium; DoA, dodecylammonium; and PEA, phenylethylammonium. LT and HT stand for low and high temperature phase, respectively.

Compound	c_0 at LT (μeV/T^2)	c_0 at HT (μeV/T^2)	μ (m_e)
$(BA)_2PbI_4$	0.13[41]–0.17[15]	0.32[41]	0.22[15]
$(BA)_2(MA)_1Pb_2I_7$	0.4[15]	...	0.216[15]
$(BA)_2(MA)_2Pb_3I_{10}$	0.79[15]	...	0.2[15]
$(BA)_2(MA)_3Pb_4I_{13}$	1.04[15]	...	0.196[15]
$(HA)_2Pb_4I_4$	...	0.33[41]	...
$(OA)_2Pb_4I_4$	0.11[41]	0.32[41]	...
$(DA)_2PbI_4$	0.16[41]	...	0.18[74]
$(DoA)_2PbI_4$	...	0.285[41]	...
$(PEA)_2PbI_4$	0.36–0.46[66,67]	...	0.087–0.091[66,67]
$(PEA)_2(MA)_1Pb_2I_7$	1.24[67]	...	0.090[67]
$(PEA)_2(MA)_2Pb_3I_{10}$	1.98[67]	...	0.103[67]
$(PEA)_2SnI_4$	0.68[66]	...	0.055[66]

Table I). Correspondingly, the authors observed a decrease in the effective mass from 0.221 to 0.186 going from $n = 1$ to $n = 5$, as summarized in Fig. 2(f). Interestingly, even for $n = 5$ the reduced mass of exciton μ is much larger than the reduced mass of the exciton in bulk MAPbI$_3$ ($\mu = 0.104$[59,61,62]). These measurements have been performed at 4 K, thus addressing only the problem of the exciton reduced mass of the low temperature phase of (BA)$_2$(MA)$_{n-1}$Pb$_n$I$_{3n+1}$.[78] In another work, the direct measurement of the diamagnetic coefficient enabled to unveil the change of the exciton reduced mass of 2D perovskites with spacers consisting of aliphatic chains of increasing length [(C$_m$H$_{2m+1}$NH$_3$)$_2$PbI$_4$ with varying m] upon structural phase transition.[41] In this work, it has been demonstrated that the length of the organic spacer has a vanishingly small effect on the diamagnetic coefficient, which instead increases by an almost a factor three between the low and the high temperature crystal phases, as seen from Table I. This considerable enhancement has been attributed to a change of the exciton reduced mass upon structural phase transition, as also suggested by band structure calculations.[41] By inspecting Table I, one realizes also that 2D perovskites with an aromatic spacer, such as phenylethylammonium (PEA), have consistently larger diamagnetic coefficients than the layered perovskites of the same thickness with an aliphatic spacer. This can be ascribed to the larger spatial extension of the exciton wavefunction in layered perovskites with an aromatic spacer due to a smaller dielectric mismatch between the well and the barrier than that of 2D perovskites with aliphatic spacers.[16] Moreover, the aromatic spacers introduces smaller structural distortions of the inorganic sublattice, which leads to consistently smaller effective masses in 2D perovskites with aromatic spacers than those with aliphatic spacers.[66,67]

The spectroscopy of interband Landau level transitions provides the most direct access to the exciton reduced mass. In the presence of a magnetic field, charge carriers are subject to cyclotron motion in a plane perpendicular to the applied magnetic field, which leads to a change of their energy and the density of states. In the parabolic band approximation, the cyclotron motion results in an extra energy E of band edge states of electrons and holes: $E = (n + 1/2)eB/m^*_{e,h}$, where n is an integer and represents the principal quantum number and $m_{e,h}$ denotes the effective mass of the electrons and holes, respectively. In 2D systems, in a magnetic field, the density of states changes from step-like to singular.[73] The orthogonality of Landau states implies that only transitions between states having the same principal quantum number are optically allowed [a schematic representation of these transitions is shown in Fig. 2(c)]. Thus, transitions between Landau levels result in a series of evenly spaced features above the bandgap, separated by $eB/m^*_h + eB/m^*_e = eB/\mu$ [see Fig. 2(d)]. This relationship provides a straightforward dependence between the energy of interband Landau level transitions and the reduced mass of the exciton. Taking into account also the energy of the bandgap, the transition energy between Landau levels as a function of magnetic field B is

$$E_N(B) = E_g + \left(N + \frac{1}{2}\right)\hbar\omega_c, \qquad (3)$$

where E_g is the single particle bandgap and $\hbar\omega_c = \frac{eB}{\mu}$. In Eq. (3), the contribution from the Zeeman energy is neglected. The different interband Landau level transitions can be summarized in a fan chart, as that of Fig. 2(e), which summarizes the observed interband Landau

level transitions in a (PEA)$_2$PbI$_4$ sample. The experimental observation of the linear dispersion of the interband Landau levels enables the accurate determination of the effective mass without any *a priori* assumption. Unlike the diamagnetic shift, which does not depend on the average time interval between two scattering events τ_{scat}, to observe Landau level transitions, the condition $\omega_c\tau_{scat} > 1$ has to be fulfilled.[73] This requires high quality samples and/or very high magnetic fields, and only very recently the observation of interband Landau level transitions has been reported for PEA$_2$PbI$_4$, PEA$_2$SnI$_4$[66] [magnetotransmission spectra shown in Fig. 2(d) and energy chart of the Landau levels reproduced in Fig. 2(e)] and (PEA)$_2$MA$_{n-1}$Pb$_n$I$_{3n+1}$.[67] The corresponding reduced exciton mass values are summarized in Table I. The importance of these results is related not only to the fact that they represent the first observation of interband Landau level transitions in 2D perovskites. Surprisingly, the reduced mass of these 2D perovskites is lower than that of the corresponding bulk perovskites MAPbI$_3$ and FASnI$_3$ for which μ is 0.104 and 0.102, respectively.[59,61,66] This is in contrast with the observation made for (BA)$_2$(MA)$_{n-1}$Pb$_n$I$_{3n+1}$[15] and points to the dominant impact of the organic spacers on the band structure dispersion. The electronic states of the organic spacers do not contribute directly to the band edge states.[45] Nevertheless, they influence the electronic properties of 2D perovskites by controlling the overlap of the metal and halide ions via structural distortions. However, so far this influence has manifested only as a change of the bandgap.[45,79] The apparently contradictory dependencies of the reduced mass on the thickness of the metal halide slabs can be reconciled by assuming that also the carrier effective mass can be tuned via structural distortions.[15,41,66,67] Notably, the fact that the reduced mass can be tuned both below and above the bulk values is in contrast with previous results obtained in the case of fully inorganic epitaxial quantum wells.[80–82] Finally, the independent determination of the reduced mass has been used to quantify the spatial extension of the exciton wave function for PEA based 2D perovskites.[67]

The observation of the Landau level dispersion allows also to precisely determine the single particle bandgap E_g because all Landau levels extrapolate to E_g at zero magnetic field.[63,66] The direct determination of the bandgap from linear absorption spectra might be highly inaccurate if the excited exciton states merge with the bandgap transition into a broad spectral feature, which results in an underestimation of the bandgap value and of the exciton binding energy.[66]

The investigation of the exciton states in high magnetic field clarifies also the origin of the complex line shape of the absorption spectrum of 2D perovskites.[46,49,69] The multiple peak structure has been so far attributed to vibronic progression[41,46,69] or distinct excitonic (polaritonic) states.[49,50,83] The results of magnetoabsorption studies of (PEA)$_2$(CH$_3$NH$_3$)$_{n-1}$Pb$_n$I$_{3n+1}$ (for $n = 1, 2, 3$)[84] and (C$_m$H$_{2m+1}$NH$_3$)$_2$PbI$_4$ (for $m = 4, 6, 8, 10, 12$)[41] support the vibronic progression scenario.[41,46,69] All the absorption spectral features are separated by around ~40 meV in (PEA)$_2$(CH$_3$NH$_3$)$_{n-1}$Pb$_n$I$_{3n+1}$ and ~15 meV in (C$_m$H$_{2m+1}$NH$_3$)$_2$PbI$_4$. The identical magnetic field induced shifts of the side peaks, as shown in Fig. 3,[66] strongly support their vibronic progression origin. This is the expected behavior of phonon replicas given that, if the lattice vibrations are unaffected by the magnetic field, all phonon assisted transitions should follow the evolution of the zero phonon line. If the side peaks originated from distinct excitonic states due to the spin–orbit coupling, or exchange interaction, they should exhibit different shifts in magnetic field, as
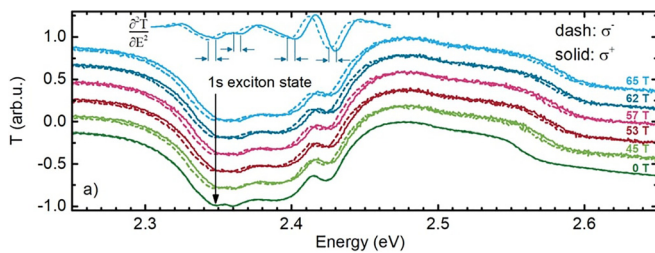
FIG. 3. Transmission spectra of (PEA)$_2$PbI$_4$ at 2 K for different magnetic fields. σ^+ and σ^- denote right- and left-handed circular polarizations. The inset shows the second derivative, highlighting the equal magnitude of the energy shift of the excitonic features. The maxima of the second derivative spectrum correspond to the minima visible in the transmission spectrum. Both the dips of the transmission spectrum and the peaks of second derivative shift by the same value with magnetic field. Adapted with permission from Dyksik et al., ACS Energy Lett. 5, 3609–3616 (2020).[66] Copyright 2020 American Chemical Society.

exemplified by the opposite shift of exchange-interaction split bright excitonic states induced by the magnetic field.[85]

Excitons—electron–hole pairs correlated by Coulomb interaction—possess a rich energy level structure, referred to as an exciton fine structure, which depends on the individual spins of the electron and the hole. The fine structure is of paramount importance to understand the interaction of excitonic complexes with light and reflects the underlying symmetry of the crystal and of the quantum confinement. The energy structure of band edge excitons in 2D perovskites[86] is very similar to that of their 3D counterparts.[87,88] Metal halide perovskites display an unusual, "inverted" band structure, which is strongly influenced by a considerably strong spin–orbit coupling in the conduction band and crystal field.[89] The states of band edge excitons are built from s-like hole states and p-like electron states with total angular momentum $J = 1/2$.[86,87] The presence of electron-hole exchange interaction results in an exciton fine structure where the ground state is a $J = 0$ optically dark (ϕ^1) state and a threefold degenerate, optically active state with total angular momentum $J = 1$, which lies at higher energy.[90] In 2D perovkites, the lack of the symmetry in the z direction further lifts the degeneracy of $J = 1$ states, which yields two degenerate states with $J_z = \pm 1$ ($\phi^{3\pm}$) and one with $J_z = 0$ (ϕ^2). The pair of degenerate states has a dipole moment in the xy plane of the crystal and couples to left- or right-handed circularly polarized light, while the latter state has a dipole moment perpendicular to the metal-halide octahedra plane (z). In the case of broken in-plane symmetry, the degeneracy of the $J_z = \pm 1$ state is completely lifted. This results in two excitonic states with a perpendicular in plane dipole orientation ($\phi^{X/Y}$), which couple to linearly polarized light. A schematic representation of the fine structure of the exciton is illustrated in Fig. 4(a).[86] The exciton fine structure in the case of 2D perovskites is analogous to that observed in 3D perovskites in tetragonal and orthorhombic phases,[85,88,91] with the notable difference that the enhanced Coulomb interaction is expected to lead to a much larger splitting of the states.[92] The splitting between the bright and dark states is expected to be in the range of a few to few tens of millielectronvolts,[93,94] one or two orders of magnitude larger than in bulk semiconductors.[85,88]

Quantifying the splitting between dark and bright states is important not only from a fundamental viewpoint, but also for the practical implementation of perovskite-based light sources. A large bright-dark

exciton splitting might be detrimental for lighting applications. It can prevent efficient thermal mixing of both states even at room temperature, thus reducing the efficiency of the light emitting device. Recent experiments suggest however that this negative aspect can be partially mitigated by the soft nature of perovskites, which determines a slow exciton relaxation to the low energy dark exciton, due to the weak coupling of exciton with acoustic phonons.[95–97] A detailed knowledge of exciton and phonon energy spectrum is crucial to understand the fundamental mechanisms which may limit the performance of 2D perovskites in light emitting applications.

Considering that half the exciton states are optically inactive in the standard experimental back scattering geometry, accessing the full exciton fine structure can be an experimentally challenging task. The ϕ^1 and ϕ^2 excitons are dipole forbidden under the light propagation in the direction perpendicular to the metal-halide plane. The ϕ^2 state can be optically accessible by moving the optical axis of the detected signal off the direction perpendicular to the quantum well[98] or by using a high numerical aperture objective,[99] but the lowest dark state remains inaccessible by the means of simplest optical measurements.

The magnetic field induces a mixing of the dark and the bright states, thereby providing a comprehensive picture of the exciton fine structure.[100] This magnetic-field mediated transfer of oscillator strength from the dipole allowed to the dipole forbidden transitions gives a direct optical access to dark states. In the same experiment, the magnetic field dependence of the exciton transition energies enables a direct measurement of carriers' g-factors, spin–orbit splitting, or crystal field.[69,90,91,100]

For a magnetic field applied in Faraday configuration, i.e., $\mathbf{E} \perp \mathbf{c}$, $\mathbf{B} \parallel \mathbf{c}$, $\mathbf{k} \parallel \mathbf{c}$, the exciton Hamiltonian H_F can be written in the basis of the zero field states as

$$H_F = \begin{bmatrix} E^1 & \gamma B & 0 & 0 \\ \gamma B & E^2 & 0 & 0 \\ 0 & 0 & E^{3+} + \delta B & 0 \\ 0 & 0 & 0 & E^{3-} - \delta B \end{bmatrix}, \quad (4)$$

where δ and γ are coefficients dependent on electron and hole g-factors, spin–orbit coupling, and crystal field.[69,90,91,100] The eigenstates of H_F are summarized in Table II. In the Faraday configuration, ϕ^1 mixes with ϕ^2 as shown in Table II, where the coefficient $a_{1,2}$ and $b_{1,2}$ depend on $\mathbf{B}$, the spin–orbit coupling, the crystal field, and the energy difference between the states ϕ^1 and ϕ^2.[86,90,91] In the high field limit, both $a_{1,2}$ and $b_{1,2}$ reach the value of $\sqrt{2}/2$, which means that the oscillator strength is equally distributed between the states ϕ_F^1, and ϕ_F^2. At the same time, the two bright in-plane exciton states experience a Zeeman splitting linear in the magnetic field. This simple energy dependence neglects the diamagnetic shift[15,41] and the possible splitting of $\phi^{3\pm}$ at 0 field due to broken in-plane symmetry.[85,94] The energy shifts of excitonic states in magnetic field in principle enable the independent determination of electron and hole g-factors since they depend on the sum (in plane) and difference (out of plane) of electron and hole g-factors. However, because the completely dark state ϕ^1 mixes only with ϕ^2, the dipoles of $\phi_F^{1,2}$ states are aligned along the z axis and their observation can be challenging and would require the collection with a high numerical aperture objective.
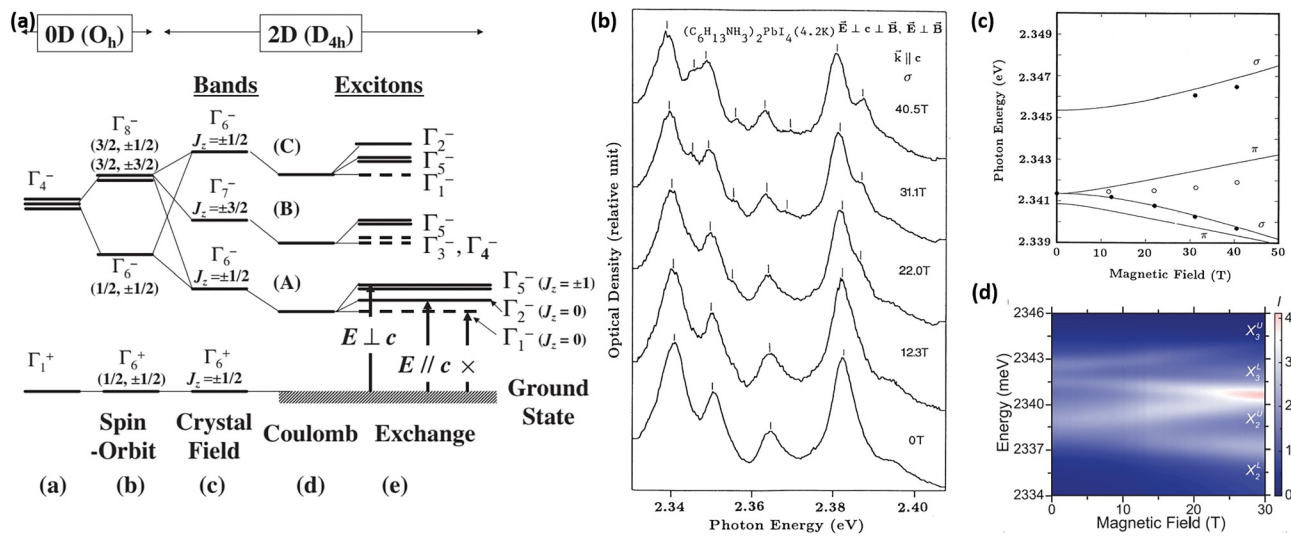
FIG. 4. (a) Evolution of the energy levels of the exciton manifold in a 2D perovskite shown by gradually introducing spin–orbit coupling, crystal field, and Coulomb and exchange interaction. Adapted with permission from Tanaka *et al.*, Jpn. J. Appl. Phys., Part 1 44, 5923 (2005).[86] Copyright 2005 The Japanese Society of Applied Physics. (b) Magnetoabsorption spectra measured in the Voigt configuration for σ polarization of $(HA)_2PbI_4$. (c) Magnetic field dependence of the lowest energy exciton states of $(HA)_2PbI_4$. Adapted with permission from Kataoka *et al.*, Phys. Rev. B 47, 2010 (1993).[69] Copyright 1993 American Physical Society. (d) False color plot of the unpolarized PL intensity of $(PEA)_2PbI_4$ for magnetic fields up to 30 T. Adapted with permission from Do *et al.*, Nano Lett. 20, 5141–5148 (2020).[94] Copyright 2020 American Chemical Society.

To optically access $\phi^{1,2}$, the Voigt configuration ($\mathbf{E}\perp\mathbf{c}$, $\mathbf{B}\perp\mathbf{c}$, $\mathbf{k}\parallel\mathbf{c}$) is beneficial. The effective Hamiltonian in this case reads for $\mathbf{B}=(B,0,0)$

$$H_V = \begin{bmatrix} E^1 & 0 & -\xi B & \xi B \\ 0 & E^2 & \eta B & \eta B \\ -\xi B & \eta B & E^3 & 0 \\ \xi B & \eta B & 0 & E^3 \end{bmatrix}. \quad (5)$$

In the Voigt configuration, the in-plane states mix with dark and out of plane states (see Table II). It is convenient to introduce so-called longitudinal $\phi^{3L} = 1/\sqrt{2}(\phi^{3+} - \phi^{3-})$ and transverse $\phi^{3T} = 1/\sqrt{2}$ $(\phi^{3+} + \phi^{3-})$ in plane states, which have dipoles aligned along x and y directions. The magnetic field transfers the oscillator strength from $\phi^{L,T}$ to $\phi^{1,2}$ and these states can be observed under π ($\mathbf{E}\parallel\mathbf{x}$) and σ ($\mathbf{E}\parallel\mathbf{y}$) linear polarizations. The mixing parameters are approximately proportional to $1/\Delta E_{ij}$, where ΔE_{ij} is energy difference between the

states. Due to the strong Coulomb interaction between electrons and holes, it is expected that ΔE_{ij} is in the range of single to few tens of meV.[93,101] Therefore, for the magnetic field-induced mixing of excitonic states to provide an experimentally detectable effect, extremely intense magnetic fields in the range of a few tens of tesla should be used.[101] This may explain why the exciton fine structure of 2D perovskites has not been conclusively elucidated so far.

In spite of these experimental challenges, there have been some reports which studied quantitatively the fine structure of exciton states of 2D perovskites. A splitting of the order of 30 meV has been measured from the PL spectrum of $(C_4H_9NH_3)_2PbBr_4$.[93] This observation has been attributed to the concomitant breakdown of selection rules in the presence of crystal distortion, higher-order transition moment processes, and phonon-assisted transitions. More recently, a 2 meV fine-structure splitting of bright exciton states in $(PEA)_2PbI_4$ has been reported, as shown in Fig. 4(d).[94] This splitting has been attributed to a broken in-plane symmetry in this 2D perovskite. So far, this is the largest splitting between bright exciton states reported for two-

TABLE II. Eigenstates of excitons in Faraday and Voigt configuration.

Faraday	Voigt
$\phi_F^{1,2} = a_{1,2}\phi^1 + b_{1,2}\phi^2$	$\phi_V^{1,3L} = c_{1,3L}\phi^1 + d_{1,3L}(\phi^{3+} - \phi^{3-})$
$E_F^{1,2} = \frac{1}{2}[(E^1 + E^2) \pm \sqrt{(E^1 - E^2)^2 + (g_{e\parallel} - g_{h\parallel})^2\mu_B^2 B^2}]$	$E_V^{1,3L} = \frac{1}{2}[(E^1 + E^3) \pm \sqrt{(E^3 - E^1)^2 + (g_{e\parallel} - g_{h\parallel})^2\mu_B^2 B^2}]$
$\mathbf{E}\parallel\mathbf{z}$	$\mathbf{E}\parallel\mathbf{x}$
$\phi_F^{3\pm} = \phi^{3\pm}$	$\phi_V^{2,3T} = c_{2,3T}\phi^2 + d_{2,3T}(\phi^{3+} + \phi^{3-})$
$E_F^{3\pm} = E^3 \pm (g_{e\parallel} + g_{h\parallel})\mu_B B$	$E_V^{2,3T} = \frac{1}{2}[(E^2 + E^3) \pm \sqrt{(E^3 - E^2)^2 + (g_{e\parallel} + g_{h\parallel})^2\mu_B^2 B^2}]$
$\mathbf{E}\parallel\mathbf{xy}$	$\mathbf{E}\parallel\mathbf{y}$

dimensional semiconducting systems. Interestingly, the authors of this work report four bright exciton states. This observation cannot be explained in the excitonic picture discussed above and presented in Fig. 4(a). A direct observation of dark states of A_2PbI_4 or A_2SnI_4 has not yet been reported. An indirect approach to accessing the energy difference between optically active and inactive levels relies on the influence of the thermal activation of the dark exciton population to the bright states on the PL spectrum and dynamics.[102] By making use of this method, a 10 meV splitting has been estimated for $(PEA)_2Pb(Sn)I_4$.[103,104] There is only one report where a high magnetic field in the Voigt configuration (up to 40 T) has been applied to study 2D perovskites.[69] The authors of this work observe the appearance of new features in the absorption spectra for magnetic fields larger than 30 T, as shown in Fig. 4(b). The energy shift analysis of π and σ polarized states with the equations presented in Table II reveals a bright dark splitting of the order of only $\sim$1 meV in $(C_6H_{13}NH_3)_2PbI_4$[69] (see Fig. 4(c)[69]). This value is significantly lower than what recently reported for other 2D perovskites,[94] as discussed above. The complex line shape of the absorption spectrum of $(C_6H_{13}NH_3)_2PbI_4$ could hinder a precise determination of the fine structure of the exciton manifold. This motivates additional studies to unveil the exciton fine structure in 2D perovskites.

The use of high magnetic field has enabled to elucidate some of the fundamental electronic properties of 2D perovskites. Many open questions could benefit from the application of high magnetic field. A question which could be addressed is the accurate measurement of the effective mass of electron and holes, which could be achieved by THz spectroscopy in magnetic fields. However, for this method to be viable, free carriers should be injected in 2D perovskites, for example, by performing above bandgap illumination.[105] Another aspect which should be clarified is whether magneto-optical experiments allow us to access the bare carrier mass or whether they can probe the polaron mass.[73] Because of the ionic character of the perovskite crystal, a strong coupling of charge carriers to optical phonons is expected.[106,107] At relatively low magnetic fields, the effective mass is in fact the polaron mass, which is larger than the bare carrier mass by a factor of $1 + \alpha/6$,[108] where α is the Frölich coupling constant. In high field limit, instead, when the phonon frequency is much lower than the cyclotron frequency, the motion of the carrier decouples from the lattice vibrations and the quantity probed by magneto-optical techniques is expected to be the bare carrier mass.[73] In the intermediate range, when $\hbar\omega_c$ approaches energy of the longitudinal optical (LO) phonon, the interaction between electrons and LO phonons resonantly increases, which results in an anti-crossing between the $N = 0$ Landau levels with one LO phonon and the $N = 1$ Landau level with no LO phonon.[109,110] The experimental observation of this effect would be a very elegant proof of the polaronic nature of carriers in perovskite compounds. A potentially interesting candidate for this experiment would be $(PEA)_2SnI_4$ due to its low effective mass.[66]

Another interesting problem, which might be addressed by magneto-optical spectroscopy, is the anisotropy of exciton wave function related to the in-plane and out of plane directions. So far, only the exciton size in the in-plane direction has been determined for 2D perovskites.[67] However, there is a lack of information concerning the penetration depth of the exciton wave function into the organic barriers. This information might be helpful to explain why in some 2D perovskites the excitons seem to couple to vibration modes localized in the organic spacers,[46,84,111] while in other compounds this does not occur.[41,112] We can imagine at least two approaches to reveal the out-of-plane exciton size. One requires the use of the Faraday geometry. In this case, the plane of the inorganic layers should be parallel to the magnetic field and the light emitted/transmitted/reflected from the edge of structure should be analyzed. This could be challenging from the experimental point of view; however, the analysis should be relatively simple by making use of Eq. (1). Alternatively, the Voigt geometry could be used, which might be easier experimentally. However, the more complex dependence of the transition energies (see Table II) can make the precise determination of diamagnetic coefficient, which should be added to the Zeeman splitting, difficult to achieve.

Finally the successful synthesis of phase pure 2D perovskites with $n > 1$[113,114] would enable the investigation of the evolution of the FSS in 2D perovskites with different inorganic slab thickness. For this purpose, the magnetic field represents the ideal experimental tool. The recent progress made in optical spectroscopy in extreme magnetic fields[115–117] together with the continuous improvement in the crystal synthesis represents a fertile ground for successful studies and to deepen our understanding of the fundamental physics of 2D perovskites.

DATA AVAILABILITY

Data sharing is not applicable to this article as no new data were created or analyzed in this study.

REFERENCES

[1]A. R. Chakhmouradian and P. M. Woodward, "Celebrating 175 years of perovskite research: A tribute to Roger H. Mitchell," Phys. Chem. Miner. **41**, 387–391 (2014).

[2]A. K. Jena, A. Kulkarni, and T. Miyasaka, "Halide perovskite photovoltaics: Background, status, and future prospects," Chem. Rev. **119**, 3036–3103 (2019).

[3]H. L. Wells, "Über die cäsium-und kalium-bleihalogenide," Z. Anorg. Chem. **3**, 195–210 (1893).

[4]D. Weber, "$CH_3NH_3PbX_3$, ein Pb (II)-system mit kubischer perowskitstruktur/$CH_3NH_3PbX_3$, a Pb (II)-system with cubic perovskite structure," Z. Naturforsch. B **33**, 1443–1445 (1978).

[5]V. M. Goldschmidt, "Die gesetze der krystallochemie," Naturwissenschaften **14**, 477–485 (1926).

[6]C. C. Stoumpos, D. H. Cao, D. J. Clark, J. Young, J. M. Rondinelli, J. I. Jang, J. T. Hupp, and M. G. Kanatzidis, "Ruddlesden–Popper hybrid lead iodide perovskite 2D homologous semiconductors," Chem. Mater. **28**, 2852–2867 (2016).

[7]D. B. Mitzi, "Synthesis, crystal structure, and optical and thermal properties of $(C_4H_9NH_3)_2MI_4$ (M = Ge, Sn, Pb)," Chem. Mater. **8**, 791–800 (1996).

[8]L. Mao, W. Ke, L. Pedesseau, Y. Wu, C. Katan, J. Even, M. R. Wasielewski, C. C. Stoumpos, and M. G. Kanatzidis, "Hybrid Dion–Jacobson 2D lead iodide perovskites," J. Am. Chem. Soc. **140**, 3775–3783 (2018).

[9]Y. Chen, Y. Sun, J. Peng, J. Tang, K. Zheng, and Z. Liang, "2D Ruddlesden–Popper perovskites for optoelectronics," Adv. Mater. **30**, 1703487 (2018).

[10]D. B. Straus and C. R. Kagan, "Electrons, excitons, and phonons in two-dimensional hybrid perovskites: Connecting structural, optical, and electronic properties," J. Phys. Chem. Lett. **9**, 1434–1447 (2018).

[11]Y.-H. Kim, H. Cho, J. H. Heo, T.-S. Kim, N. Myoung, C.-L. Lee, S. H. Im, and T.-W. Lee, "Multicolored organic/inorganic hybrid perovskite light-emitting diodes," Adv. Mater. **27**, 1248–1254 (2015).

[12]N. Rytova, "Coulomb interaction of electrons in a thin film," Dokl. Akad. Nauk **163**, 1118–1120 (1965).

[13]L. Keldysh, "Coulomb interaction in thin semiconductor and semimetal films," Sov. J. Exp. Theor. Phys. Lett. **29**, 658 (1979).

[14]T. Ishihara, J. Takahashi, and T. Goto, "Optical properties due to electronic transitions in two-dimensional semiconductors $(C_nH_{2n+1}NH_3)_2PbI_4$," Phys. Rev. B **42**, 11099 (1990).

[15]J.-C. Blancon, A. V. Stier, H. Tsai, W. Nie, C. C. Stoumpos, B. Traore, L. Pedesseau, M. Kepenekian, F. Katsutani, G. Noe, J. Kono, S. Tretiak, S. Crooker, C. Katan, M. Kanatzidis, J. Crochet, J. Even, and A. Mohite, "Scaling law for excitons in 2D perovskite quantum wells," Nat. Commun. **9**, 2254 (2018).

[16]X. Hong, T. Ishihara, and A. Nurmikko, "Dielectric confinement effect on excitons in pbi 4-based layered semiconductors," Phys. Rev. B **45**, 6961 (1992).

[17]D. B. Mitzi, C. Feild, W. Harrison, and A. Guloy, "Conducting tin halides with a layered organic-based perovskite structure," Nature **369**, 467–469 (1994).

[18]C. Kagan, D. Mitzi, and C. Dimitrakopoulos, "Organic-inorganic hybrid materials as semiconducting channels in thin-film field-effect transistors," Science **286**, 945–947 (1999).

[19]K. S. Novoselov, A. K. Geim, S. V. Morozov, D. Jiang, Y. Zhang, S. V. Dubonos, I. V. Grigorieva, and A. A. Firsov, "Electric field effect in atomically thin carbon films," Science **306**, 666–669 (2004).

[20]K. F. Mak, C. Lee, J. Hone, J. Shan, and T. F. Heinz, "Atomically thin MoS_2: A new direct-gap semiconductor," Phys. Rev. Lett. **105**, 136805 (2010).

[21]T. T. Tran, K. Bray, M. J. Ford, M. Toth, and I. Aharonovich, "Quantum emission from hexagonal boron nitride monolayers," Nat. Nanotechnol. **11**, 37–41 (2016).

[22]C. R. Dean, L. Wang, P. Maher, C. Forsythe, F. Ghahari, Y. Gao, J. Katoch, M. Ishigami, P. Moon, M. Koshino, T. Taniguchi, K. Watanabe, K. Shepard, and P. Kim, "Hofstadter's butterfly and the fractal quantum Hall effect in moiré superlattices," Nature **497**, 598–602 (2013).

[23]P. Rivera, K. L. Seyler, H. Yu, J. R. Schaibley, J. Yan, D. G. Mandrus, W. Yao, and X. Xu, "Valley-polarized exciton dynamics in a 2D semiconductor heterostructure," Science **351**, 688–691 (2016).

[24]I. C. Smith, E. T. Hoke, D. Solis-Ibarra, M. D. McGehee, and H. I. Karunadasa, "A layered hybrid perovskite solar-cell absorber with enhanced moisture stability," Angew. Chem. Int. Ed. **53**, 11232–11235 (2014).

[25]H. Tsai, W. Nie, J.-C. Blancon, C. C. Stoumpos, R. Asadpour, B. Harutyunyan, A. J. Neukirch, R. Verduzco, J. J. Crochet, S. Tretiak, L. Pedesseau, J. Even, M. A. Alam, G. Gupta, J. Lou, P. M. Ajayan, M. J. Bedzyk, M. G. Kanatzidis, and A. G. Mohite, "High-efficiency two-dimensional Ruddlesden–Popper perovskite solar cells," Nature **536**, 312–316 (2016).

[26]X. Zhang, X. Ren, B. Liu, R. Munir, X. Zhu, D. Yang, J. Li, Y. Liu, D.-M. Smilgies, R. Li, Z. Yang, T. Niu, X. Wang, A. Amassiam, K. Zhao, and S. Liu, "Stable high efficiency two-dimensional perovskite solar cells via cesium doping," Energy Environ. Sci. **10**, 2095–2102 (2017).

[27]C. Liang, D. Zhao, Y. Li, X. Li, S. Peng, G. Shao, and G. Xing, "Ruddlesden–Popper perovskite for stable solar cells," Energy Environ. Mater. **1**, 221–231 (2018).

[28]D. Bryant, N. Aristidou, S. Pont, I. Sanchez-Molina, T. Chotchunangatchaval, S. Wheeler, J. R. Durrant, and S. A. Haque, "Light and oxygen induced degradation limits the operational stability of methylammonium lead triiodide perovskite solar cells," Energy Environ. Sci. **9**, 1655–1660 (2016).

[29]T. A. Berhe, W.-N. Su, C.-H. Chen, C.-J. Pan, J.-H. Cheng, H.-M. Chen, M.-C. Tsai, L.-Y. Chen, A. A. Dubale, and B.-J. Hwang, "Organometal halide perovskite solar cells: Degradation and stability," Energy Environ. Sci. **9**, 323–356 (2016).

[30]T. Niu, J. Lu, X. Jia, Z. Xu, M.-C. Tang, D. Barrit, N. Yuan, J. Ding, X. Zhang, Y. Fan, T. Luo, Y. Zhang, D. M. Smilgies, Z. Liu, A. Amassian, S. Jin, K. Zhao, and S. Liu, "Interfacial engineering at the 2D/3D heterojunction for high-performance perovskite solar cells," Nano Lett. **19**, 7181–7190 (2019).

[31]J. Byun, H. Cho, C. Wolf, M. Jang, A. Sadhanala, R. H. Friend, H. Yang, and T.-W. Lee, "Efficient visible quasi-2D perovskite light-emitting diodes," Adv. Mater. **28**, 7515–7520 (2016).

[32]X. Yang, X. Zhang, J. Deng, Z. Chu, Q. Jiang, J. Meng, P. Wang, L. Zhang, Z. Yin, and J. You, "Efficient green light-emitting diodes based on quasi-two-dimensional composition and phase engineered perovskite with surface passivation," Nat. Commun. **9**, 570 (2018).

[33]H. Zhang, Q. Liao, Y. Wu, Z. Zhang, Q. Gao, P. Liu, M. Li, J. Yao, and H. Fu, "2D Ruddlesden–Popper perovskites microring laser array," Adv. Mater. **30**, 1706186 (2018).

[34]C. Qin, A. S. Sandanayaka, C. Zhao, T. Matsushima, D. Zhang, T. Fujihara, and C. Adachi, "Stable room-temperature continuous-wave lasing in quasi-2D perovskite films," Nature **585**, 53–57 (2020).

[35]E. R. Dohner, A. Jaffe, L. R. Bradshaw, and H. I. Karunadasa, "Intrinsic white-light emission from layered hybrid perovskites," J. Am. Chem. Soc. **136**, 13154–13157 (2014).

[36]E. R. Dohner, E. T. Hoke, and H. I. Karunadasa, "Self-assembly of broadband white-light emitters," J. Am. Chem. Soc. **136**, 1718–1721 (2014).

[37]W. Fu, J. Wang, L. Zuo, K. Gao, F. Liu, D. S. Ginger, and A.K.-Y. Jen, "Two-dimensional perovskite solar cells with 14.1% power conversion efficiency and 0.68% external radiative efficiency," ACS Energy Lett. **3**, 2086–2093 (2018).

[38]Z. Tan, Y. Wu, H. Hong, J. Yin, J. Zhang, L. Lin, M. Wang, X. Sun, L. Sun, Y. Huang, K. Liu, Z. Liu, and H. Peng, "Two-dimensional $(C_4H_9NH_3)_2PbBr_4$ perovskite crystals for high-performance photodetector," J. Am. Chem. Soc. **138**, 16612–16615 (2016).

[39]K. Wang, C. Wu, D. Yang, Y. Jiang, and S. Priya, "Quasi-two-dimensional halide perovskite single crystal photodetector," ACS Nano **12**, 4919–4929 (2018).

[40]A. Fieramosca, L. Polimeno, V. Ardizzone, L. De Marco, M. Pugliese, V. Maiorano, M. De Giorgi, L. Dominici, G. Gigli, D. Gerace, D. Ballarini, and D. Sanvitto, "Two-dimensional hybrid perovskites sustaining strong polariton interactions at room temperature," Sci. Adv. **5**, eaav9967 (2019).

[41]M. Baranowski, S. J. Zelewski, M. Kepenekian, B. Traoré, J. M. Urban, A. Surrente, K. Galkowski, D. K. Maude, A. Kuc, E. P. Booker, R. Kudrawiec, S. D. Stranks, and P. Plochocka, "Phase-transition-induced carrier mass enhancement in 2D Ruddlesden–Popper perovskites," ACS Energy Lett. **4**, 2386–2392 (2019).

[42]J. A. Sichert, A. Hemmerling, C. Cardenas-Daw, A. S. Urban, and J. Feldmann, "Tuning the optical bandgap in layered hybrid perovskites through variation of alkyl chain length," APL Mater. **7**, 041116 (2019).

[43]L. Lanzetta, J. M. Marin-Beloqui, I. Sanchez-Molina, D. Ding, and S. A. Haque, "Two-dimensional organic tin halide perovskites with tunable visible emission and their use in light-emitting devices," ACS Energy Lett. **2**, 1662–1668 (2017).

[44]M. P. Hautzinger, D. Pan, A. K. Pigg, Y. Fu, D. J. Morrow, M. Leng, M.-Y. Kuo, N. Spitha, D. P. Lafayette, D. D. Kohler, J. C. Wright, and S. Jin, "Band edge tuning of two-dimensional Ruddlesden–Popper perovskites by A cation size revealed through nanoplates," ACS Energy Lett. **5**, 1430–1437 (2020).

[45]J. L. Knutson, J. D. Martin, and D. B. Mitzi, "Tuning the band gap in hybrid tin iodide perovskite semiconductors using structural templating," Inorg. Chem. **44**, 4699–4705 (2005).

[46]D. B. Straus, S. Hurtado Parra, N. Iotov, J. Gebhardt, A. M. Rappe, J. E. Subotnik, J. M. Kikkawa, and C. R. Kagan, "Direct observation of electron–phonon coupling and slow vibrational relaxation in organic–inorganic hybrid perovskites," J. Am. Chem. Soc. **138**, 13798–13801 (2016).

[47]L. Mao, Y. Wu, C. C. Stoumpos, B. Traore, C. Katan, J. Even, M. R. Wasielewski, and M. G. Kanatzidis, "Tunable white-light emission in single-cation-templated three-layered 2D perovskites $(CH_3CH_2NH_3)_4Pb_3Br_{10-x}Cl_x$," J. Am. Chem. Soc. **139**, 11956–11963 (2017).

[48]L. Mao, Y. Wu, C. C. Stoumpos, M. R. Wasielewski, and M. G. Kanatzidis, "White-light emission and structural distortion in new corrugated two-dimensional lead bromide perovskites," J. Am. Chem. Soc. **139**, 5210–5215 (2017).

[49]S. Neutzner, F. Thouin, D. Cortecchia, A. Petrozza, C. Silva, and A. R. S. Kandada, "Exciton-polaron spectral structures in two-dimensional hybrid lead-halide perovskites," Phys. Rev. Mater. **2**, 064605 (2018).

[50]F. Thouin, D. A. Valverde-Chávez, C. Quarti, D. Cortecchia, I. Bargigia, D. Beljonne, A. Petrozza, C. Silva, and A. R. S. Kandada, "Phonon coherences reveal the polaronic character of excitons in two-dimensional lead halide perovskites," Nat. Mater. **18**, 349–356 (2019).

[51]T. Matsushima, S. Hwang, A. S. Sandanayaka, C. Qin, S. Terakawa, T. Fujihara, M. Yahiro, and C. Adachi, "Solution-processed organic–inorganic perovskite field-effect transistors with high hole mobilities," Adv. Mater. **28**, 10275–10281 (2016).

[52]T. Matsushima, F. Mathevet, B. Heinrich, S. Terakawa, T. Fujihara, C. Qin, A. S. Sandanayaka, J.-C. Ribierre, and C. Adachi, "N-channel field-effect transistors with an organic-inorganic layered perovskite semiconductor," Appl. Phys. Lett. **109**, 253301 (2016).

[53]F. Liu, L. Wang, J. Wang, F. Wang, Y. Chen, S. Zhang, H. Sun, J. Liu, G. Wang, Y. Hu, and C. Jiang, "2D Ruddlesden–Popper perovskite single crystal field-effect transistors," Adv. Funct. Mater. **31**, 2005662 (2021).

[54]B. Fallahazad, H. C. Movva, K. Kim, S. Larentis, T. Taniguchi, K. Watanabe, S. K. Banerjee, and E. Tutuc, "Shubnikov–de Haas oscillations of high-mobility holes in monolayer and bilayer WSe_2: Landau level degeneracy, effective mass, and negative compressibility," Phys. Rev. Lett. **116**, 086601 (2016).

[55]R. J. Nicholas, "The magnetophonon effect," Prog. Quantum Electron. **10**, 1–75 (1985).

[56]R. Dexter, H. Zeiger, and B. Lax, "Cyclotron resonance experiments in silicon and germanium," Phys. Rev. **104**, 637 (1956).

[57]C. Liu, S. Lin, D. Tsui, H. Lee, and D. Ackley, "Cyclotron resonance measurements of electron effective mass in strained AlGaAs/InGaAs/GaAs pseudomorphic structures," Appl. Phys. Lett. **53**, 2510–2512 (1988).

[58]J. Maan, G. Belle, A. Fasolino, M. Altarelli, and K. Ploog, "Magneto-optical determination of exciton binding energy in $GaAs$-$Ga_{1-x}Al_xAs$ quantum wells," Phys. Rev. B **30**, 2253 (1984).

[59]A. Miyata, A. Mitioglu, P. Plochocka, O. Portugall, J. T.-W. Wang, S. D. Stranks, H. J. Snaith, and R. J. Nicholas, "Direct measurement of the exciton binding energy and effective masses for charge carriers in organic–inorganic tri-halide perovskites," Nat. Phys. **11**, 582–587 (2015).

[60]Z. Yang, A. Surrente, K. Galkowski, N. Bruyant, D. K. Maude, A. A. Haghighirad, H. J. Snaith, P. Plochocka, and R. J. Nicholas, "Unraveling the exciton binding energy and the dielectric constant in single-crystal methylammonium lead triiodide perovskite," J. Phys. Chem. Lett. **8**, 1851–1855 (2017).

[61]Z. Yang, A. Surrente, K. Galkowski, A. Miyata, O. Portugall, R. Sutton, A. Haghighirad, H. J. Snaith, D. Maude, P. Plochocka, and R. Nicholas, "Impact of the halide cage on the electronic properties of fully inorganic cesium lead halide perovskites," ACS Energy Lett. **2**, 1621–1627 (2017).

[62]A. M. Soufiani, Z. Yang, T. Young, A. Miyata, A. Surrente, A. Pascoe, K. Galkowski, M. Abdi-Jalebi, R. Brenes, J. Urban, N. Zhang, V. Bulovic, O. Portugall, Y.-B. Cheng, R. J. Nicholas, A. Ho-Baillie, M. A. Green, P. Plochocka, and S. D. Stranks, "Impact of microstructure on the electron–hole interaction in lead halide perovskites," Energy Environ. Sci. **10**, 1358–1366 (2017).

[63]K. Galkowski, A. Surrente, M. Baranowski, B. Zhao, Z. Yang, A. Sadhanala, S. Mackowski, S. D. Stranks, and P. Plochocka, "Excitonic properties of low-band-gap lead–tin halide perovskites," ACS Energy Lett. **4**, 615–621 (2019).

[64]M. Baranowski and P. Plochocka, "Excitons in metal-halide perovskites," Adv. Energy Mater. **10**, 1903659 (2020).

[65]M. Baranowski, P. Plochocka, R. Su, L. Legrand, T. Barisien, F. Bernardot, Q. Xiong, C. Testelin, and M. Chamarro, "Exciton binding energy and effective mass of $CsPbCl_3$: A magneto-optical study," Photonics Res. **8**, A50–A55 (2020).

[66]M. Dyksik, H. Duim, X. Zhu, Z. Yang, M. Gen, Y. Kohama, S. Adjokatse, D. K. Maude, M. A. Loi, D. A. Egger, M. Baranowski, and P. Plochocka, "Broad tunability of carrier effective masses in two-dimensional halide perovskites," ACS Energy Lett. **5**, 3609–3616 (2020).

[67]M. Dyksik, S. Wang, W. Paritmongkol, D. K. Maude, W. A. Tisdale, M. Baranowski, and P. Plochocka, "Tuning the excitonic properties of the 2D $(PEA)_2(MA)_{n-1}$ Pb_nI_{3n+1} perovskite family via quantum confinement," J. Phys. Chem. Lett. **12**, 1638–1643 (2021).

[68]C.-Q. Xu, H. Sakakura, T. Kondo, S. Takeyama, N. Miura, Y. Takahashi, K. Kumata, and R. Ito, "Magneto-optical effects of excitons in $(C_{10}H_{21}NH_3)_2PbI_4$ under high magnetic fields up to 40 T," Solid State Commun. **79**, 249–253 (1991).

[69]T. Kataoka, T. Kondo, R. Ito, S. Sasaki, K. Uchida, and N. Miura, "Magneto-optical study on excitonic spectra in $(C_6H_{13}NH_3)_2PbI_4$," Phys. Rev. B **47**, 2010 (1993).

[70]M. Hirasawa, T. Ishihara, T. Goto, S. Sasaki, K. Uchida, and N. Miura, "Magnetoreflection of the lowest exciton in a layered perovskite-type compound $(C_{10}H_{21}NH_3)_2PbI_4$," Solid State Commun. **86**, 479–483 (1993).

[71]A. Chernikov, T. C. Berkelbach, H. M. Hill, A. Rigosi, Y. Li, O. B. Aslan, D. R. Reichman, M. S. Hybertsen, and T. F. Heinz, "Exciton binding energy and nonhydrogenic Rydberg series in monolayer WS_2," Phys. Rev. Lett. **113**, 076802 (2014).

[72]A. V. Stier, N. P. Wilson, K. A. Velizhanin, J. Kono, X. Xu, and S. A. Crooker, "Magnetooptics of exciton Rydberg states in a monolayer semiconductor," Phys. Rev. Lett. **120**, 057405 (2018).

[73]N. Miura, *Physics of Semiconductors in High Magnetic Fields* (Oxford University Press, 2008), Vol. 15.

[74]K. Tanaka, T. Takahashi, T. Kondo, T. Umebayashi, K. Asai, and K. Ema, "Image charge effect on two-dimensional excitons in an inorganic-organic quantum-well crystal," Phys. Rev. B **71**, 045312 (2005).

[75]B. Traore, L. Pedesseau, L. Assam, X. Che, J.-C. Blancon, H. Tsai, W. Nie, C. C. Stoumpos, M. G. Kanatzidis, S. Tretiak, A. D. Mohite, J. Even, M. Kepenekian, and C. Katan, "Composite nature of layered hybrid perovskites: Assessment on quantum and dielectric confinements and band alignment," ACS Nano **12**, 3321–3332 (2018).

[76]D. Feldstein, R. Perea-Causin, S. Wang, M. Dyksik, K. Watanabe, T. Taniguchi, P. Plochocka, and E. Malic, "Microscopic picture of electron–phonon interaction in two-dimensional halide perovskites," J. Phys. Chem. Lett. **11**, 9975–9982 (2020).

[77]D. Sapori, M. Kepenekian, L. Pedesseau, C. Katan, and J. Even, "Quantum confinement and dielectric profiles of colloidal nanoplatelets of halide inorganic and hybrid organic–inorganic perovskites," Nanoscale **8**, 6369–6378 (2016).

[78]D. G. Billing and A. Lemmerer, "Synthesis, characterization and phase transitions in the inorganic–organic layered perovskite-type hybrids, $[(C_nH_{2n+1}NH_3)_2PbI_4]$, n = 4, 5 and 6," Acta Crystallogr., Sect. B **63**, 735–747 (2007).

[79]L. Pedesseau, D. Sapori, B. Traore, R. Robles, H.-H. Fang, M. A. Loi, H. Tsai, W. Nie, J.-C. Blancon, A. Neukirch, S. Tretiak, A. D. Mohite, C. Katan, J. Even, and M. Kepenekian, "Advances and promises of layered halide hybrid perovskite semiconductors," ACS Nano **10**, 9776–9786 (2016).

[80]B. Nag and S. Mukhopadhyay, "In-plane effective mass in narrow quantum wells of nonparabolic semiconductors," Appl. Phys. Lett. **62**, 2416–2418 (1993).

[81]C. Wetzel, R. Winkler, M. Drechsler, B. Meyer, U. Rössler, J. Scriba, J. Kotthaus, V. Härle, and F. Scholz, "Electron effective mass and nonparabolicity in $Ga_{0.47}In_{0.53}As/InP$ quantum wells," Phys. Rev. B **53**, 1038 (1996).

[82]M. Städele and K. Hess, "Effective-mass enhancement and nonparabolicity in thin GaAs quantum wells," J. Appl. Phys. **88**, 6945–6947 (2000).

[83]F. Thouin, D. Cortecchia, A. Petrozza, A. R. S. Kandada, and C. Silva, "Enhanced screening and spectral diversity in many-body elastic scattering of excitons in two-dimensional hybrid metal-halide perovskites," Phys. Rev. Res. **1**, 032032 (2019).

[84]J. M. Urban, G. Chehade, M. Dyksik, M. Menahem, A. Surrente, G. Trippé-Allard, D. K. Maude, D. Garrot, O. Yaffe, E. Deleporte, P. Plochocka, and M. Baranowski, "Revealing excitonic phonon coupling in $(PEA)_2(MA)_{n-1}$ Pb_nI_{3n+1} 2D layered perovskites," J. Phys. Chem. Lett. **11**, 5830–5835 (2020).

[85]M. Baranowski, K. Galkowski, A. Surrente, J. Urban, Ł. Kłopotowski, S. Maćkowski, D. K. Maude, R. Ben Aich, K. Boujdaria, M. Chamarro, C. Testelin, P. K. Nayak, M. Dollman, H. J. Snaith, R. J. Nicholas, and P. Plochocka, "Giant fine structure splitting of the bright exciton in a bulk $MAPbBr_3$ single crystal," Nano Lett. **19**, 7054–7061 (2019).

[86]K. Tanaka, T. Takahashi, T. Kondo, K. Umeda, K. Ema, T. Umebayashi, K. Asai, K. Uchida, and N. Miura, "Electronic and excitonic structures of inorganic–organic perovskite-type quantum-well crystal $(C_4H_9NH_3)_2PbBr_4$," Jpn. J. Appl. Phys., Part 1 **44**, 5923 (2005).

[87]K. Tanaka, T. Takahashi, T. Ban, T. Kondo, K. Uchida, and N. Miura, "Comparative study on the excitons in lead-halide-based perovskite-type

crystals $CH_3NH_3PbBr_3$ $CH_3NH_3PbI_3$," Solid State Commun. **127**, 619–623 (2003).

[88] M. Fu, P. Tamarat, H. Huang, J. Even, A. L. Rogach, and B. Lounis, "Neutral and charged exciton fine structure in single lead halide perovskite nanocrystals revealed by magneto-optical spectroscopy," Nano Lett. **17**, 2895–2901 (2017).

[89] J. Even, L. Pedesseau, J.-M. Jancu, and C. Katan, "Importance of spin–orbit coupling in hybrid organic/inorganic perovskites for photovoltaic applications," J. Phys. Chem. Lett. **4**, 2999–3005 (2013).

[90] Z. Yu, "Effective-mass model and magneto-optical properties in hybrid perovskites," Sci. Rep. **6**, 28576 (2016).

[91] J. Ramade, L. M. Andriambariarijaona, V. Steinmetz, N. Goubet, L. Legrand, T. Barisien, F. Bernardot, C. Testelin, E. Lhuillier, A. Bramati, and M. Chamarro, "Fine structure of excitons and electron–hole exchange energy in polymorphic $CsPbBr_3$ single nanocrystals," Nanoscale **10**, 6393–6401 (2018).

[92] M. Maialle, E. d. A. e Silva, and L. Sham, "Exciton spin dynamics in quantum wells," Phys. Rev. B **47**, 15776 (1993).

[93] K. Ema, K. Umeda, M. Toda, C. Yajima, Y. Arai, H. Kunugita, D. Wolverson, and J. Davies, "Huge exchange energy and fine structure of excitons in an organic-inorganic quantum well material," Phys. Rev. B **73**, 241310 (2006).

[94] T. T. H. Do, A. Granados del Aguila, D. Zhang, J. Xing, S. Liu, M. Prosnikov, W. Gao, K. Chang, P. C. Christianen, and Q. Xiong, "Bright exciton fine-structure in two-dimensional lead halide perovskites," Nano Lett. **20**, 5141–5148 (2020).

[95] K. Xu, J. F. Vliem, and A. Meijerink, "Long-lived dark exciton emission in Mn-doped $CsPbCl_3$ perovskite nanocrystals," J. Phys. Chem. C **123**, 979–984 (2019).

[96] M. Fu, P. Tamarat, J.-B. Trebbia, M. I. Bodnarchuk, M. V. Kovalenko, J. Even, and B. Lounis, "Unraveling exciton–phonon coupling in individual $FAPbI_3$ nanocrystals emitting near-infrared single photons," Nat. Commun. **9**, 3318 (2018).

[97] P. Tamarat, M. I. Bodnarchuk, J.-B. Trebbia, R. Erni, M. V. Kovalenko, J. Even, and B. Lounis, "The ground exciton state of formamidinium lead bromide perovskite nanocrystals is a singlet dark state," Nat. Mater. **18**, 717–724 (2019).

[98] Y. Huo, V. Křápek, O. Schmidt, and A. Rastelli, "Spontaneous brightening of dark excitons in GaAs/AlGaAs quantum dots near a cleaved facet," Phys. Rev. B **95**, 165304 (2017).

[99] C. Robert, T. Amand, F. Cadiz, D. Lagarde, E. Courtade, M. Manca, T. Taniguchi, K. Watanabe, B. Urbaszek, and X. Marie, "Fine structure and lifetime of dark excitons in transition metal dichalcogenide monolayers," Phys. Rev. B **96**, 155423 (2017).

[100] M. Bayer, G. Ortner, O. Stern, A. Kuther, A. Gorbunov, A. Forchel, P. Hawrylak, S. Fafard, K. Hinzer, T. Reinecke, S. Walck, J. Reithmaier, F. Klopf, and F. Schäfer, "Fine structure of neutral and charged excitons in self-assembled In(Ga)As/(Al)GaAs quantum dots," Phys. Rev. B **65**, 195315 (2002).

[101] X.-X. Zhang, T. Cao, Z. Lu, Y.-C. Lin, F. Zhang, Y. Wang, Z. Li, J. C. Hone, J. A. Robinson, D. Smirnov, S. G. Louie, and T. F. Heinz, "Magnetic brightening and control of dark excitons in monolayer WSe_2," Nat. Nanotechnol. **12**, 883–888 (2017).

[102] E. V. Shornikova, L. Biadala, D. R. Yakovlev, V. F. Sapega, Y. G. Kusrayev, A. A. Mitioglu, M. V. Ballottin, P. C. Christianen, V. V. Belykh, M. V. Kochiev,

N. N. Sibeldin, A. A. Golovatenko, A. V. Rodina, N. A. Gippius, A. Kuntzmann, Y. Jiang, M. Nasilowski, B. Dubertret, and M. Bayer, "Addressing the exciton fine structure in colloidal nanocrystals: The case of CdSe nanoplatelets," Nanoscale **10**, 646–656 (2018).

[103] H.-H. Fang, J. Yang, S. Adjokatse, E. Tekelenburg, M. E. Kamminga, H. Duim, J. Ye, G. R. Blake, J. Even, and M. A. Loi, "Band-edge exciton fine structure and exciton recombination dynamics in single crystals of layered hybrid perovskites," Adv. Funct. Mater. **30**, 1907979 (2020).

[104] G. Folpini, D. Cortecchia, A. Petrozza, and A. R. S. Kandada, "The role of a dark exciton reservoir in the luminescence efficiency of two-dimensional tin iodide perovskites," J. Mater. Chem. C **8**, 10889–10896 (2020).

[105] M. Keshavarz, S. Wiedmann, H. Yuan, E. Debroye, M. Roeffaers, and J. Hofkens, "Light-and temperature-modulated magneto-transport in organic–inorganic lead halide perovskites," ACS Energy Lett. **3**, 39–45 (2018).

[106] J. Yin, H. Li, D. Cortecchia, C. Soci, and J.-L. Bredas, "Excitonic and polaronic properties of 2d hybrid organic–inorganic perovskites," ACS Energy Lett. **2**, 417–423 (2017).

[107] K. Miyata, D. Meggiolaro, M. T. Trinh, P. P. Joshi, E. Mosconi, S. C. Jones, F. De Angelis, and X.-Y. Zhu, "Large polarons in lead halide perovskites," Sci. Adv. **3**, e1701217 (2017).

[108] R. P. Feynman, "Slow electrons in a polar crystal," Phys. Rev. **97**, 660 (1955).

[109] S. Najda, H. Yokoi, S. Takeyama, N. Miura, and P. Pfeffer, "Infrared magneto-spectroscopy of n-type InP at magnetic fields up to 150 T," Phys. Rev. B **44**, 1087 (1991).

[110] S. Najda, S. Takeyama, N. Miura, P. Pfeffer, and W. Zawadzki, "Infrared magnetospectroscopy of GaAs at magnetic fields up to 150 T," Phys. Rev. B **40**, 6189 (1989).

[111] D. B. Straus, S. Hurtado Parra, N. Iotov, Q. Zhao, M. R. Gau, P. J. Carroll, J. M. Kikkawa, and C. R. Kagan, "Tailoring hot exciton dynamics in 2D hybrid perovskites through cation modification," ACS Nano **14**, 3621–3629 (2020).

[112] C. M. Mauck, A. France-Lanord, A. C. Hernandez Oendra, N. S. Dahod, J. C. Grossman, and W. A. Tisdale, "Inorganic cage motion dominates excited-state dynamics in 2D-layered perovskites $(C_xH_{2x+1}NH_3)_2PbI_4$ (x = 4–9)," J. Phys. Chem. C **123**, 27904–27916 (2019).

[113] Y. Tong, E. Bladt, M. F. Aygüler, A. Manzi, K. Z. Milowska, V. A. Hintermayr, P. Docampo, S. Bals, A. S. Urban, L. Polavarapu, and J. Feldmann, "Highly luminescent cesium lead halide perovskite nanocrystals with tunable composition and thickness by ultrasonication," Angew. Chem. Int. Ed. **55**, 13887–13892 (2016).

[114] Y. Hu, L. M. Spies, D. Alonso-Álvarez, P. Mocherla, H. Jones, J. Hanisch, T. Bein, P. R. Barnes, and P. Docampo, "Identifying and controlling phase purity in 2D hybrid perovskite thin films," J. Mater. Chem. A **6**, 22215–22225 (2018).

[115] J. Béard, J. Billette, N. Ferreira, P. Frings, J.-M. Lagarrigue, F. Lecouturier, and J.-P. Nicolin, "Design and tests of the 100-T triple coil at LNCMI," IEEE Trans. Appl. Supercond. **28**, 1–5 (2018).

[116] R. Battesti, J. Beard, S. Böser, N. Bruyant, D. Budker, S. A. Crooker, E. J. Daw, V. V. Flambaum, T. Inada, I. G. Irastorza, F. Karbstein, D. L. Kim, M. G. Kozlov, Z. Melhem, A. Phipps, P. Pugnat, G. Rikken, C. Rizzo, M. Schott, Y. K. Semertzidis, H. H. ten Kate, and G. Zavattini, "High magnetic fields for fundamental physics," Phys. Rep. **765–766**, 1–39 (2018).

[117] D. Nakamura, A. Ikeda, H. Sawabe, Y. Matsuda, and S. Takeyama, "Record indoor magnetic field of 1200 t generated by electromagnetic flux-compression," Rev. Sci. Instrum. **89**, 095106 (2018).